Estimating the compressional and shear wave speeds of a shallow water seabed from the vertical coherence of ambient noise in the water column

Nicholas M. Carbone, Grant B. Deane, and Michael J. Buckingham
Marine Physical Laboratory, Scripps Institution of Oceanography, University of California at San Diego, 9500 Gilman Drive, La Jolla, California 92093-0704

(Received 25 March 1997; accepted for publication 15 September 1997)

Due to the multiple bottom reflections encountered in shallow water environments, the spatial structure of the ambient noise field depends strongly on the geoacoustic properties of the seabed, which are invariant over time scales associated with most measurements. The vertical directionality and coherence are relatively stable features of the noise that are determined primarily by the seabed, rather than temporal variations in the surface source distribution. In this paper, estimates of the compressional and shear wave speeds are determined from ambient noise measurements over shear supporting seabeds. Using a model of wind-generated noise over an elastic seabed, it is shown that the noise is sensitive to the compressional and shear wave speeds in the upper few meters of seabed. An inversion procedure is developed based on a matched field of the complex, broadband coherence from a single hydrophone pair. Using ambient noise data from two shear supporting sites, compressional and shear wave estimates are obtained that are in good agreement with independent surveys. For one site where the bedrock is exposed, a half-space model of the seabed yields reasonable estimates of the seabed parameters. For the other site, the presence of a thin sedimentary layer results in a low estimate from the half-space model. However, when the layer is included in the model, the estimates of the underlying bedrock are in good agreement with a seismic survey.
 [S0001-4966(98)05101-7]

PACS numbers: 43.30.Ma, 43.30.Pc [DLB]

INTRODUCTION

In shallow water, sound interacts strongly with the seabed. Sound emanating from a source undergoes multiple reflections between the sea surface and sea floor. The ambient noise field is a stochastic process of many such noise sources and the respective interactions of their wave fields with the environmental boundaries. As a consequence of the multipath interaction, the time-averaged ambient noise exhibits spatial structure that is largely determined by the characteristics of the seabed. In particular, the geoacoustic parameters of the seabed determine the relative reflection versus refraction of sound from the water column into the seabed as a function of grazing angle. In turn, this relationship affects the vertical directionality and vertical coherence of the ambient noise. These functions of the noise can therefore be measured in the ocean environment, and used to estimate the seabed parameters.

The dependence of the vertical directionality and coherence was examined by Chapman[1] who modeled typical variations in the noise structure for seabeds ranging from silt to chalk, and demonstrated good agreement of the real component of the coherence with data from two shallow water sites. Based on the seabed's effect on the vertical coherence, Buckingham and Jones[2] used a low-loss, fluid model to estimate the compressional wave speed from experimental measurements of the noise. In the present study, this idea is developed further to address shear-supporting seabed types. The dependencies of the ambient noise on the reflective properties of the seabed are presented and subsequently used to invert for the compressional and shear wave speeds using the vertical coherence of the noise.

The inversion is based on the broadband vertical coherence from a single hydrophone pair. It utilizes the frequency band of 100 Hz to a few kilo-Hertz, where ambient noise often contains contributions from both natural source mechanisms and anthropogenic sources. The present study focuses solely on wind/wave-generated noise, which can be modeled as a uniform distribution of surface sources. Undoubtedly, other noise sources, particularly ships, can be important in many shallow water areas. These sources often have variable spatial distributions, and thus very different vertical noise structure compared to wind noise. The present study constitutes an initial investigation into the somewhat ideal situation where wind noise, which has a predictable spatial distribution, is the dominant source mechanism.

In this paper, the dominant environmental effects on the noise field are examined and used to estimate the compressional and shear wave speeds from ambient noise data. A normal mode model of wind-generated ambient noise over a shear-supporting basement is developed in Sec. I. In Sec. II, the noise is examined in terms of the narrowband vertical directionality and, alternatively, the broadband vertical coherence. The directionality is used because it is physically intuitive, whereas the coherence, which is easier to measure, forms the basis of the inversion. The fundamental effects of the seabed on the noise field are examined using a homogeneous half-space seabed. Then, a layered seabed is used to investigate the seabed penetration depth characterized by the broadband coherence. Finally, the effect of a sound speed

profile on the coherence is addressed. In Sec. III, ambient noise data are presented in order to demonstrate the stationarity of the noise field coherence with regard to temporally varying aspects of the ocean environment. In Sec. IV, the inversion procedure is introduced and subsequently applied to ambient noise data from two shear-supporting sites in Sec. V.

I. AMBIENT NOISE MODEL FOR A SHALLOW WATER DUCT OVER A SHEAR-SUPPORTING BASEMENT

Several models of ambient noise are currently in existence. A review of these models can be found in a paper by Hamson.[3] One such model for the spatial correlation in the vertical was developed by Buckingham.[4] This model accounts for uncorrelated omnidirectional noise sources over a low-loss, fluid basement in an isovelocity shallow water channel. The low-loss approximation made by Buckingham allowed for the continuous spectrum, which is often attributed to a branch line integral and can be difficult to compute, to be omitted from the calculation. However, as this energy represents the contribution from nearby sources, it can be an important component of the wind-generated ambient noise.[5] A more general formulation, which allows for the continuous spectrum component, was expressed in the form of a wave number integral by Kuperman and Ingenito.[6] This general expression is evaluated using the fast field program (FFP) OASES.[7,8] Recently, Harrison[9] has shown that equivalent results may also be obtained using a simple ray approach.

In this section, recent developments in the area of eigenvalue finding routines[10] are incorporated with these previous approaches in order to express the entire wind-generated ambient noise field as a sum of normal modes. The expression accounts for lossy, elastic seabeds, and it incorporates the discrete and continuous spectra by including the trapped and leaky modes. It can be computed quickly and accurately for the isovelocity case and used to examine the seabed effects on the noise field.

The physical model is shown in Fig. 1. The wind noise generators are modeled as a plane of omnidirectional point sources which are Poisson distributed in space and time and are located just below a pressure release surface. The water column contains a sound speed c_{p1} and density ρ_1. The seabed consists of an optional fluid layer of variable thickness overlying an elastic half-space. The parameters for the layer are the compressional wave speed and attenuation, c_{p2} and α_{p2}, and the density ρ_2. The parameters for the half-space are the compressional wave speed and attenuation, c_{p3} and α_{p3}; shear wave speed and attenuation, c_{s3} and α_{s3}; and the density ρ_3. A sensor array, shown as a single receiver pair, is located in the water column away from the interfaces.

The goal is to describe the second-order statistics as a function of the seabed parameters. To do this, the cross-spectral density between receivers will be expressed in terms of the Green's function, which in turn depends on the seabed parameters. The cross-spectral density will then be used to compute the vertical directionality and the vertical coherence, which will help to interpret the seabed's effect on the noise field.

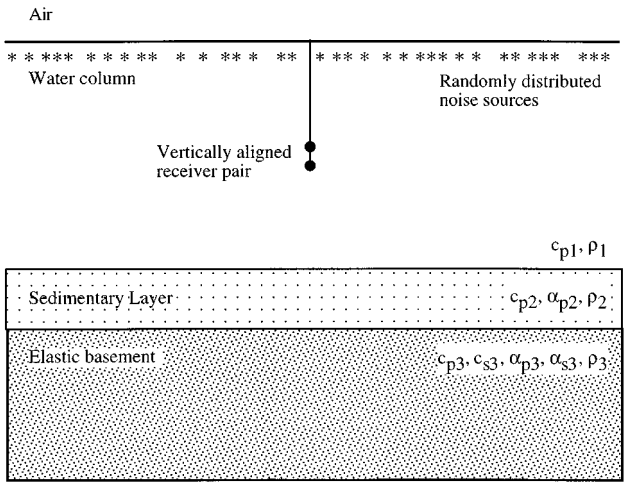

FIG. 1. Canonical shallow water ambient noise model showing an optional fluid layer of variable thickness and the viscoelastic parameters of the seabed half-space. The cross-spectral density between the two hydrophones is calculated from a random distribution of point sources just below the pressure release surface.

Considering an incremental surface area dA as shown in Fig. 2, the expected value of the cross-spectral density for a Poisson process is given by Carson's theorem,[11] which can be expressed as

$$d\overline{S_{ij}}(\omega) = 2\nu Q^2 G(r,\omega,z_{ri}) G^*(r,\omega,z_{rj})\, dA, \tag{1}$$

where the overbar stands for ensemble average, ν is the source density per unit time, Q is the source strength, G are the Green's function at receiver depths z_{ri} and z_{rj}, ω is the angular frequency, and the asterisk denotes complex conju-

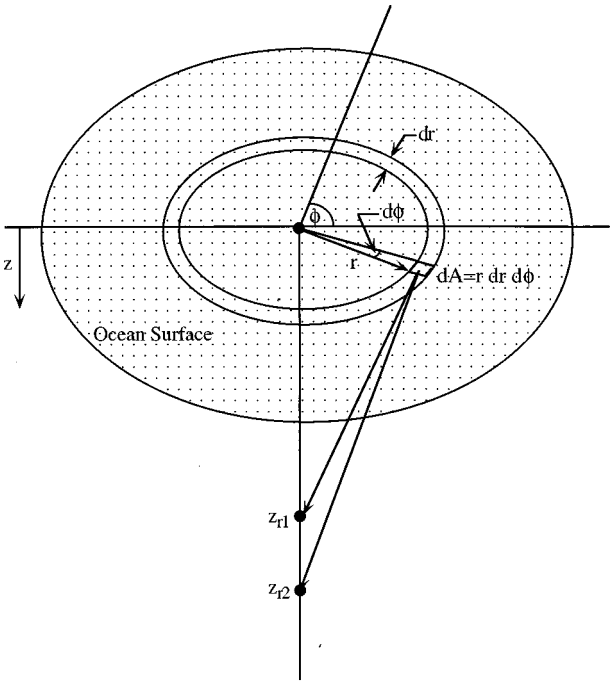

FIG. 2. Source model for the ambient noise field. The cross-spectral density of the ambient noise is derived using the Green's function within the incremental area dA and then integrating over azimuth and range.

gate. To obtain cross-spectral densities for the total surface, the incremental area $dA = r dr d\phi$ is integrated over range and angle. Assuming azimuthal symmetry, the integral over ϕ provides a factor of 2π and the resulting integral for the expected value of the total cross-spectral density is given by

$$\overline{S_{ij}}(\omega) = 4\pi\nu Q^2 \int_0^\infty r G(r,\omega,z_{ri}) G^*(r,\omega,z_{rj})\, dr. \quad (2)$$

Thus, the expected value for the average cross-spectral density of the random process is expressed in terms of the deterministic Green's functions for a given environment. Considering the shallow water duct environment of Fig. 1, the Green's function solution to the wave equation is well known and can be expressed as a sum of normal modes

$$G(r,\omega,z_r) = i\pi \sum_n \varphi_n(z_r)\varphi_n(z_s) H_0^1(k_n r), \quad (3)$$

where n is the mode number, φ_n are the mode eigenvectors evaluated at the source and receiver, and H_0^1 is a Hankel function which depends on range r and the mode eigenvalues k_n.

Substituting the Green's function from Eq. (3) into the cross-spectral density in Eq. (2) and performing the range integration results in the following double sum of normal modes:

$$\overline{S_{ij}}(\omega) = 16\pi\nu Q \sum_{n=1}^{\infty} \varphi_n(z_s)\varphi_n(z_{ri}) \sum_{m=1}^{\infty} \varphi_m^*(z_s)\varphi_m^*(z_{rj}) \times \frac{\ln(k_n/k_m^*) - i\pi}{k_m^{*2} - k_n^2}. \quad (4)$$

The upper limit of infinity in the mode sum is due to choosing the Pekeris branch cut, which results in a finite sum of trapped modes plus an infinite sum of leaky modes plus a branch line integral, which can be neglected. Because the noise sources are distributed across the entire surface, the noise field includes overhead source contributions, and the continuous spectrum is an important contributor to the total noise field. The infinite sum provides an accurate description of the noise without the necessity for computing the branch line integral. In practice the sum may be truncated at mode cutoff for a rigid bottom. This corresponds to a maximum mode number of $N_{\text{modes}} = 2fh/c_{p1}$, where f is the frequency and h is the duct depth.

Some concern was raised by Stickler[12] as to whether the mode sum derived from the Pekeris cut provides a sufficiently complete solution for the field in the water column. However, Stickler's concern over the importance of the branch line integral is based on a specific example where a single trapped mode exists and is very near cutoff. For the geometries and frequencies used in this study, many modes exist in the water column. Consequently, the branch line integral can be neglected and the Pekeris mode sum provides an accurate representation of the field in the water column.

The seabed parameters couple into the noise field solution through the reflection coefficient which determines the mode eigenvalues k_n. For the case of an isovelocity profile in the water, the eigenfunctions are sines and the eigenvalue solutions are obtained for the lossy, elastic seabed using the complex effective depth method of Zhang and Tindle.[10] By allowing for an angle-dependent complex effective depth and iterating the eigenvalue solutions,[13] the procedure provides the exact eigenvalues of both the trapped and leaky mode poles.

Once the eigenvalues have been obtained and the cross-spectral density computed, the vertical directionality may be obtained by beamsteering a multi-element array across the vertical span of the water column. To steer the array at an angle θ_s from the horizontal, the proper phase delay for a receiver at position z_i is given by

$$w_i(\theta_s) = a_i \exp\left(-i\frac{\omega z_i \sin(\theta_s)}{c_{p1}}\right), \quad (5)$$

where a_i is real-valued window weighting that may be used to provide array shading. The directional power for the angle θ_s is then the sum over all hydrophones according to the equation

$$F(\theta_s,\omega) = \sum_{i,j=1}^{Nhyd} w_i^*(\theta_s)\overline{S_{ij}}(\omega) w_j(\theta_s), \quad (6)$$

where again the asterisk denotes complex conjugate.

The vertical coherence is simply a normalized version of the cross-spectral density. It may be expressed for a variable receiver separation at a single frequency, or it may be expressed as a broadband calculation from a single receiver pair. For the purpose of this study, we desire the simplicity obtained in using a measurement from a single hydrophone pair. Consequently, the coherence is expressed as the following broadband function:

$$\Gamma_{ij}(\omega) = \frac{\overline{S_{ij}}(\omega)}{\sqrt{\overline{S_{ii}}(\omega)\overline{S_{jj}}(\omega)}}, \quad (7)$$

where $i = 1$ and $j = 2$. We note here that the coherence is a complex function, as is the cross-spectral density between the two receivers.

Having established a theoretical framework for the wind-generated ambient noise field, we can now interpret the seabed's effect on the ambient noise directionality and coherence.

II. INTERPRETING THE AMBIENT NOISE FIELD

A. Fundamental effects of a viscoelastic seabed on the ambient noise field

The ambient noise inversion will be based on the broadband coherence from a single hydrophone pair. However, as this function is not physically intuitive, the effect of the seabed on the ambient noise field will be described by first discussing the reflection coefficient, progressing to the vertical directionality, and finally arriving at the vertical coherence. The reflection coefficient describes the angular dependence of the reflection strength of a single plane wave as determined by the seabed parameters. The vertical directionality is a measurable quantity of the noise in which the properties of the reflection coefficient are manifest in the noise power per unit angle. Although the directionality has the

benefit of being easy to interpret, it has the drawback of requiring a multiple element array where the useful frequency band is limited by the minimum receiver separation. The coherence, on the other hand, requires only two elements, and its frequency band is limited only by the sampling frequency and receiver response. Consequently, the coherence has the benefits of being a simpler measurement and allowing a wider frequency band to be examined. Additionally, the use of a broadband measurement offers greater immunity to dominant shipping lines which tend to occur at lower frequencies. To relate the coherence to the vertical directionality, we will make use of the spatial Fourier transform relationship derived by Cox.[14] This relationship relates the complex coherence to the vertical directionality, whereby the real component of the coherence represents the directional symmetry in the noise, and the imaginary component represents asymmetry in the noise. Although the relationship breaks down for nonhomogeneous noise fields, it will be useful in relating the coherence to the directionality and, thus, to the seabed reflection coefficient. Homogeneous noise is not, however, a necessary condition for performing ambient noise inversions based on the coherence or the directionality. Provided that an adequate representation of the field exists, inversions can be performed by matching the theory to the measurements in the water column.

To examine the fundamental seabed effects on the noise field, we consider the case of a viscoelastic half-space without the presence of the sedimentary layer. We will consider the compressional wave speed, c_{p3}; the shear wave speed, c_{s3}; and the compressional wave attenuation, α_{p3}. Computer simulations have shown that typical variations in the remaining parameters, ρ_3 and α_{s3}, are of lesser importance in determining the spatial structure of ambient noise. Consequently, they will not be considered in this analysis.

Figure 3 shows the reflection coefficient, vertical directionality, and vertical coherence for half-space parameter combinations of $[c_{p3}, c_{s3}, \alpha_{p3}]$ as follows: I, [1700, 0.01, 0.01]; II, [2400, 0.01, 0.01]; III, [2400, 750, 0.1]; and IV, [2400, 1000, 0.1], where the wave speeds are given in units of m/s and attenuation is in dB/λ. The line types are given by: case I (-·), case II (—), case III (- -), and case IV (··).

Reflection coefficients for four seabed combinations are shown in Fig. 3(a). The effect of the compressional wave speed can be seen by comparing the solid line to the dash–dot line. The critical angle of total internal reflection derives from Snell's law which relates the refraction angle to the ratio of sound speeds at the interface. Increasing the value of c_{p2} results in an increased critical angle, and thus a larger range of angles where total internal reflection occurs. This is the most basic and dominant effect of the seabed on the acoustic wave energy. Because of the simplicity of the relationship, the critical angle is an easy identifier of the compressional wave speed.

Comparing the dashed and dotted lines to the solid line shows the result of increasing the shear wave speed in the seabed. Higher levels of shear result in decreased reflection of energy propagating at angles between grazing and the critical angle. Thus, with regard to energy in the water column, the conversion of compressional to shear waves is a loss mechanism that preferentially attenuates intermediate, subcritical angle energy.

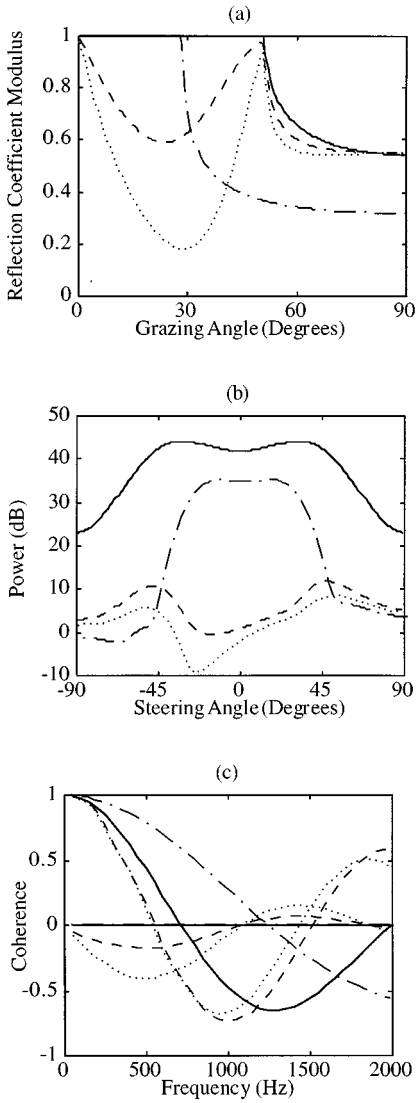

FIG. 3. The (a) reflection coefficient, (b) vertical directionality, and (c) vertical coherence are shown for varying seabed conditions. The parameters $[c_{p3}, c_{s3}, \alpha_{p3}]$ vary as follows: [1700, 0.01, 0.01], (-·); [2400, 0.01, 0.01], (—); [2400, 750, 0.1], (--); and [2400, 1000, 0.1], (··). The wave speeds are given in units of m/s and attenuation is in dB/λ.

In the absence of compressional wave attenuation, the reflection coefficient curves obtain a value of unity at the critical angle, even when shear is present. However, the presence of compressional wave attenuation decreases the reflection of critical and subcritical angle energy. Because of the compressional wave attenuation, the dashed and dotted curves in Fig. 3(a) obtain a value slightly less than unity at the critical angle.

Figure 3(b) shows the effect of the seabed parameters on the vertical directionality. The curves have been computed from an 11-hydrophone array using a Hanning window, an interelement spacing of 1.47 m, a frequency of 480 Hz, a 100-m channel, and a source strength of unity. Standard practice is to normalize these curves to absolute hydrophone level and to plot them on a polar plot. Rather than follow this

procedure, the unnormalized levels of the curves are plotted on a log-linear plot to show better the absolute effects of the loss mechanism.

It should be clear from the similarity in Fig. 3(a) and (b) that the character of the reflection coefficient manifests itself in the vertical power of the noise field. Comparing in Fig. 3(b) the solid line to the dash–dot line isolates the effect of varying the compressional wave speed. The angle span where total internal reflection occurs can be seen in the relative vertical power, where the faster compressional wave speed case has a broader peak around the horizontal. Furthermore, because a greater amount of energy has totally reflected along the multipath, the higher compressional wave speed case also has a higher absolute power level for an equal source strength.

In the dashed and dotted curves we see that the inclusion of shear results in intermediate mode stripping, creating a ''rabbit ear'' appearance to the directionality. The amount of mode stripping is dependent on the shear speed and the corresponding amount of compressional to shear wave conversion at the seabed. Because shear represents an energy loss mechanism, the directionality exhibits an asymmetry where more energy is present at upward-looking angles than at downward-looking angles. The compressional wave attenuation has a relatively minor effect on these curves, which is to clip the level of the peaks at the critical angle.

Figure 3(c) shows the complex coherence functions obtained from a 1-m receiver separation over the frequency band of 100–2000 Hz. The real part approaches unity at zero frequency; the imaginary part approaches zero. The solid and dash–dot curves demonstrate the effect of the compressional wave speed in the lossless environment. For these curves, the imaginary part is very close to zero because, for the lossless seabed, the noise field directionality is nearly symmetric about the horizontal. (A small amount of asymmetry always occurs due to penetration of high angle energy.) The effect of the compressional wave speed on the coherence is that increases in c_{p3} shift the zero crossings in the real component of the coherence to a lower frequency. In the limit, as c_{p3} becomes large, the noise field becomes isotropic (or entirely symmetric) and the zero crossing approaches a frequency of $f = c_{p1}/2s$, where s is the receiver separation.

The effect of shear can be seen in the dashed and dotted curves. Compared to the solid curves, the real coherence zero crossing frequency has decreased due to the loss of symmetry in the noise directionality. In addition, the magnitude of the imaginary component has increased due to the asymmetry associated with the intermediate mode stripping. Comparing the dashed and dotted curves indicates that these variations in the real and imaginary coherence increase with increasing shear wave speed.

In addition to shear, the compressional wave attenuation is a loss mechanism that can affect the asymmetry in the noise directionality. Although its properties differ from those of shear, attenuation can have similar effects on the vertical coherence. This raises uncertainty as to which parameter is causing the noise field asymmetry. One option would be to invert for the ''effective attenuation'' [15] which is a combination of all attenuation mechanisms including shear, attenuation, and scattering. However, it is known from numerous *in situ* studies by Hamilton[16–18] and others that fast seabeds have high shear wave speeds and low attenuation values. Consequently, the effects of attenuation from a fast, shear-supporting seabed are expected to be small. The relative effects of shear and attenuation can be seen in Fig. 4 where the coherence is plotted for parameter variations typical of a moraine seabed.[19] In Fig. 4(a) the attenuation has been varied from 0.1 to 0.5 dB/λ; in Fig. 4(b) the shear speed has been varied from 500 to 700 m/s. Comparing Fig. 4(a) and (b) shows that, for a moraine seabed, shear has a greater effect on the coherence than does the compressional wave attenuation. This will be increasingly true for progressively faster seabed types where attenuation values decrease and shear speeds increase. Consequently, typical variations in seabed attenuation should not provide significant error in the estimates of c_{p3} and c_{s3}, provided that the inversion is applied to sufficiently hard materials where shear speeds are high and attenuation is low. The presence of attenuation in unconsolidated sediments will, however, prohibit inverting for the low shear speeds associated with these materials. Therefore, we concentrate our inversions on fast, consolidated materials where shear is the dominant loss mechanism. To further minimize the error incurred in the inversion, empirically determined relationships will be used to correlate the attenua-

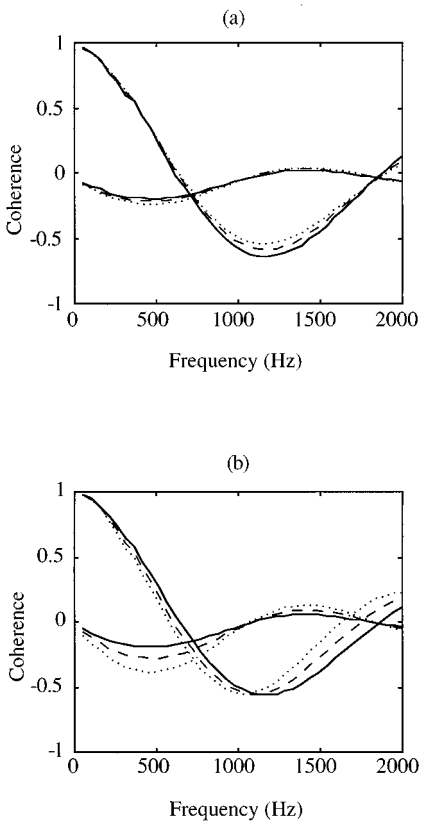

FIG. 4. The comparative effects of shear and compressional wave absorption for a moraine seabed showing (a) attenuation effects: $c_p = 2000$, $c_s = 600$, varying $\alpha_p = 0.1$ (—), 0.3 (––), 0.5 (··); and (b) shear effects: $c_p = 2000$, $\alpha_p = 0.3$, varying $c_s = 500$ (—), 600 (––), 700 (··). Sound speeds given in m/s, absorption given in dB/λ.

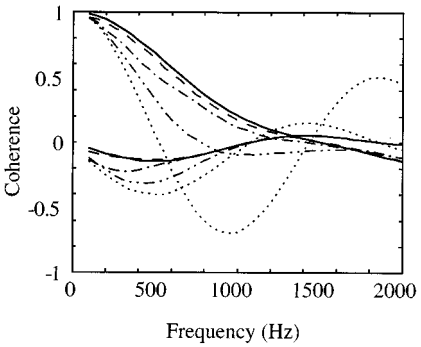

FIG. 5. The effect of a layer on the broadband coherence from a receiver pair separated by 1 m. The seabed model varies as follows: chalk half-space without a layer (··), 1-m layer of sand over chalk (-··), 2-m layer of sand over chalk (-·), 5-m layer of sand over chalk (--), and sand half-space without a layer (—). The curves indicate that the coherence is only sensitive to the upper 5 m of seabed material.

tion with the compressional wave speed. This correlation is discussed in the Appendix.

B. The penetration depth

Using ambient noise to determine seabed parameters will provide an average estimate for some finite penetration depth into the seabed. This penetration depth will depend on the acoustic wavelength of the ambient noise used in the calculation. Narrowband simulations of the vertical directionality indicate that the noise is sensitive to approximately the upper one wavelength of seabed. Consequently, for frequencies varying from 100 to 2000 Hz, a vertical footprint of 15 to 0.75 m, respectively, may be obtainable provided an array of sufficient aperture is used. However, utilizing the broadband coherence does not allow for estimates at the individual frequency components. Rather, the coherence provides a single estimate which represents an intermediate value over the penetration depths delimited by the frequency band employed in the inversion.

To illustrate the vertical footprint obtained using the noise coherence, a fluid layer of variable thickness is now included in the model. The coherence curves for a sand layer over a chalk substrate seabed are shown in Fig. 5. The hydrophone pair is separated by 1 m and located at midwater depth in a 100-m channel. The thickness of the layer varies as 1 m (-··), 2 m (-·), and 5 m (--). The limiting cases are the chalk half-space with no layer (··) and the sand half-space with no layer (—). The figure shows that the coherence is very sensitive to as little as 1 m of sediment over the chalk substrate. The curves for the three layered basements lie between the two half-space limits, representing a sort of average between the two materials. Furthermore, as the sand layer thickens, the coherence progressively approaches the sand half-space result. The coherence for the 5-m layer is barely distinguishable from the sand half-space. For the frequencies and receiver separations specified, these curves indicate that the coherence is only sensitive to the upper 5 m of seabed, and that this sensitivity is dominated by the surficial material. Consequently, the inversion technique will not be useful in determining deep sediment structure, but may provide an inexpensive means of monitoring seasonal variations in sediment overburden in shallow water areas.

C. The effect of a sound speed profile

The effect of a water column sound speed profile on the noise directionality and coherence has been considered previously by Hamson,[5] Kuperman and Ingenito,[6] and others. The presence of a sound speed profile will affect the ambient noise inversions in two ways: the noise field homogeneity and the perceived critical angle. In the isovelocity environment the noise field is approximately homogeneous away from the surface and bottom interfaces.[4] As a consequence, the precise location of the receiver pair is not an important consideration, provided that the two receivers are not too far apart and that neither is near an interface. In the presence of a sound speed profile this simplifying factor breaks down. The sound speed profile results in bent rays, or vertically constrained mode shapes, depending on one's preferred point of view. Consequently, receiver placement within the profile dictates what collection of rays or what modal amplitudes contribute to the measured field. For this reason, placement of the receivers, even within the center of the water column, becomes a consideration that can affect the inversion calculations.

The second important factor related to the sound speed profile is that the energy is preferentially bent away from the horizontal. Upon first consideration it might appear that all energy is bent more vertically and is thus more likely to exceed the critical angle of the bottom. However, the effect is actually more prevalent on the horizontally propagating energy than on the energy near the critical angle. This can be understood very simply in terms of Snell's law. Consider a ray launched from the surface in a duct containing a sound speed profile. For a launch angle θ_{surf} from the horizontal, the angle of arrival at a given hydrophone will be

$$\theta_{\text{rec}} = \cos^{-1}((c_{\text{rec}}/c_{\text{surf}})\cos\ \theta_{\text{surf}}),$$

where c_{rec} and c_{surf} are the sound speeds at the receiver and surface, respectively. For a downward-refracting profile that varies 10 m/s from the surface to the receiver, a horizontally launched ray will have an arrival angle of $\theta_{\text{rec}} = 6.6°$ whereas a ray launched at 30° will have an arrival angle of $\theta_{\text{rec}} = 30.7°$, which is a much smaller deviation. Thus, the effect of the profile is not so much to bend energy beyond the critical angle of the bottom as it is to strip energy from the horizontal.

The profile effect can also be viewed as preferential alteration in the excitation strength of the lower-order modes. A downward-refracting profile will constrain a particular mode shape to the lower portion of the water column, making the mode less excitable by near surface sources. Conversely, an upward refracting profile will constrain the mode to the upper portion of the water column, increasing its excitation strength.

This effect creates a ''noise notch'' around the horizontal in the downward refracting case, and a filling in of the notch in the upward refracting case. This is illustrated in Fig. 6 for a moraine seabed. The velocity profiles are shown in Fig. 6(a), where there are two downward-refracting, one is-

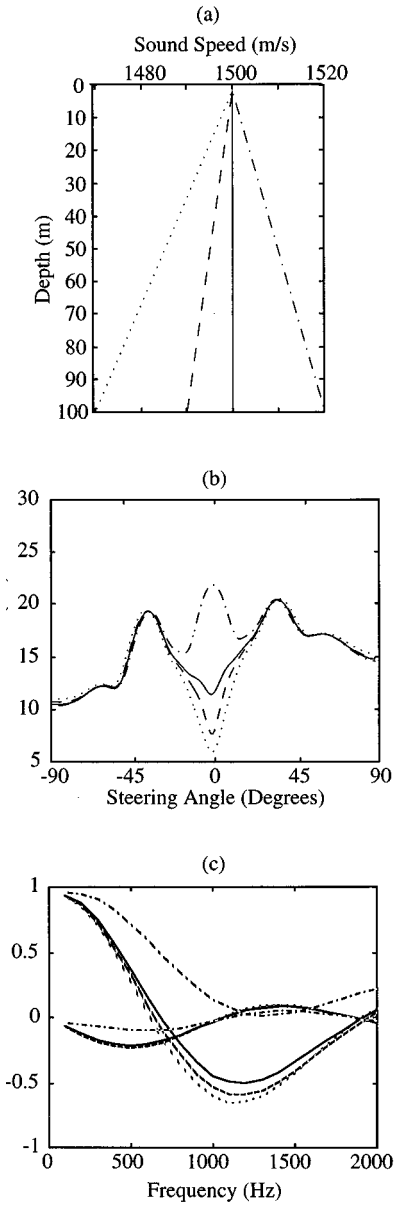

FIG. 6. The effect of a sound speed profile on the vertical directionality and the vertical coherence. (a) Sound speed profiles, (b) directionality for a moraine seabed, and (c) coherence for a moraine seabed. The line types are consistent with those given in (a).

ovelocity, and one upward-refracting profile. The line types are consistent throughout the figure, with solid representing isovelocity, dashed and dotted representing downward refracting, and the dash–dot representing upward refracting. The noise curves were calculated using OASES.[7,8] Figure 6(b) shows the directionality at 480 Hz for the an 11-element array with 1.47-m interelement spacing and a source depth of 0.1 m. The broad dip below the critical angle is due to intermediate mode stripping associated with the shear-supporting moraine seabed. In addition, a narrow notch around the horizontal is present for isovelocity and downward-refracting profiles. In the isovelocity case, the notch is due to the source dipole radiation pattern used in the OASES program. However, the depth of the notch increases depending on the severity of the profile and the corresponding decrease in the excitation of the lower-order modes. In the case of the upward refracting profile, the excitation of horizontal modes is enhanced, creating a hump around the horizontal.

The effect on the coherence of variations in the horizontal component of the noise field can be predicted by considering a purely horizontal noise component. In the case of horizontal plane wave noise there is no phase difference between two vertically separated sensors. In other words, the signals on the two sensors are perfectly coherent. Consequently, we expect enhancements in the horizontal component to increase the real coherence and drive the imaginary coherence toward zero. Conversely, notches in the horizontal component should place greater emphasis on higher-order modes, which are subject to attenuation and provide asymmetry to the directionality. This should decrease the real coherence and increase the imaginary part. This is shown in Fig. 6(c), where the vertical coherence is shown for a 1-m separated receiver pair centered at midwater depth above the moraine seabed. The noise notch associated with the downward-refracting case results in a reduced zero crossing frequency of the real coherence and a small increase in the magnitude of the imaginary coherence. In the upward-refracting case, the opposite effect is true.

Figure 6 indicates that the sound speed profile provides a measurable change in the coherence, and that including a measurement of the profile in the inversion could improve the accuracy of the inversion. In the upward-refracting case, it is clear that neglecting the profile from the inversion would result in substantial estimation error. For the downward-refracting case, however, the profile has a much smaller effect on the coherence, which remains dominated by the seabed. Consequently, only a small error will be incurred in an inversion if an isovelocity model is used when the actual *in situ* profile is downward refracting.

III. THE STATIONARITY OF THE NOISE COHERENCE

Because the ambient noise is a random process, it will naturally undergo random fluctuations over time. The use of noise in performing seabed inversions is based on the underlying tenet that the time-averaged noise coherence is a robust and repeatable measurement of the random process. Thus, the inversion assumes some level of stationarity whereby fluctuations in the coherence are of minor importance with respect to parameter estimation. Not all statistical measures of ambient noise are stationary. For instance, stationarity does not hold for the power spectral density which varies substantially with sea state. However, as the coherence is normalized with respect to the power spectral density, it is, in fact, a sufficiently stationary measurement of the random process to permit its use in the ambient noise inversion. This statement is justified below.

The broadband coherence is computed from a finite time measurement of the ambient noise field at two vertically separated receivers. Denote the time series on each receiver by $x_i(t)$ where $i=1,2$, and $X_i(f,\Delta T)$ is the corresponding finite Fourier transform over the time segment ΔT. The cross-spectral density estimate is obtained by averaging N segments, each of length ΔT, according to the following equation:

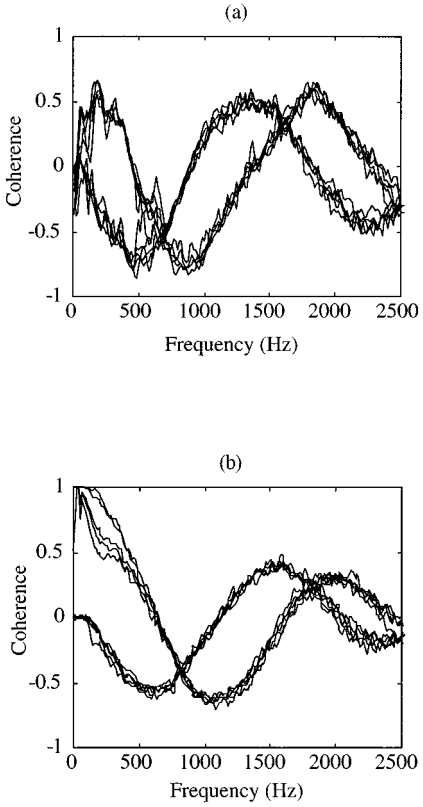

FIG. 7. The stationarity of the broadband vertical coherence is demonstrated using five individual estimates of the coherence spaced over a period of time. The coherence curves shown in (a) were obtained from the Cortes Bank using 20-s averages spaced over a 1-h period. The coherence curves shown in (b) were estimated from 40-s averages taken on five consecutive days at a site along the Florida Shelf.

$$\overline{\hat{S}_{ij}}(f) = \frac{1}{N}\sum_{n=1}^{N} X_i(f,\Delta T_n)X_j^*(f,\Delta T_n), \tag{8}$$

where the overbar stands for ensemble average and the hat indicates estimation. The coherence is then a normalized version of the cross-spectral density according to the equation

$$\hat{\Gamma}_m(f) = \frac{\overline{\hat{S}_{12}}(f)}{\sqrt{\overline{\hat{S}_{11}}(f)\,\overline{\hat{S}_{22}}(f)}}, \tag{9}$$

where $\hat{\Gamma}_m$ denotes measured coherence estimate.

In order to demonstrate the stationarity of the measured coherence, estimates obtained from two shallow water sites are shown in Fig. 7. For each site, coherence estimates are plotted from five distinct time intervals. The calculations were made using 512-point FFTs with 50% overlap and a Kaiser–Bessel[20] window with $\beta = \pi\alpha = 7.85$.

Figure 7(a) shows the coherence taken from the Cortes Bank in sea state 3. The data were digitized at a sampling frequency of 7 kHz. The five curves were obtained using relatively short 20-s averages spaced approximately equally over a 1-h measurement period. (The real coherence curves approach $+1$ at low frequency, but fall off toward zero at DC. The low-frequency falloff is attributed to flow noise which resulted from an imperfect decoupling of the array from the surface movement.) The consistency in the five curves demonstrates the relative stationarity of the noise field coherence over the 1-h period. We have found similar consistency over these timescales in data from several other shallow water sites. The Cortes Bank is particularly noteworthy because the corresponding spectral levels vary by as much as 15 dB over this measurement period, but the coherence remains stable.

In Fig. 7(b) the coherence is plotted using data from five consecutive days at a muddy sand site along the Florida Shelf. During the five-day measurement period, the sea state varied between 1 and 3 and the spectral levels varied by up to 15 dB. The data were digitized at 6.34 kHz and the coherence curves were obtained from 40-s averages. On three of the five days intermittent dropout occurred in the data. The data were interpolated through the faulty points, which caused the coherence variations below about 300 Hz. Aside from the artifact at low frequency, the coherence shows a tremendous amount of consistency over the five-day period, despite the variation in sea state and spectral levels.

These and other observations strongly suggest that the wind-generated ambient noise coherence is a stable measurement which is dominated by time-invariant properties, rather than random fluctuations in the source distribution or ocean environment. As the average coherence structure is primarily controlled by seabed reflectivity, it should provide a suitable means of inverting for seabed parameters.

IV. INVERSION PROCEDURE

The inversion is based on a simple curve fit between the theoretical and measured coherence functions. The underlying philosophy is that, since the coherence is a function of the seabed parameters, the best fit will occur when the seabed parameter values used in the model are equal to the seabed parameters occurring at the experimental site. As the coherence is a broadband, complex function, the goal is to minimize the residual between real and imaginary parts across the frequency band of interest. The norm is therefore defined as the broadband, root-mean-square (rms) difference between the theoretical and experimental coherence curves. Because the real and imaginary parts provide separate information, the difference function is a linear combination of the two rms differences (real and imaginary). This allows for the option of unequal weighting of the real and imaginary parts, as discussed below. The norm may be written as

$$\Delta(c_{p3},c_{s3},z_s) = \frac{100}{\sqrt{N}}\left\{\frac{1}{2}\sqrt{\sum_{i=1}^{N}\left[\frac{\Re(\hat{\Gamma}_m(f_i)-\Gamma_t(f_i))}{2}\right]^2} + \frac{1}{2}\sqrt{\sum_{i=1}^{N}\left[\frac{\Im(\hat{\Gamma}_m(f_i)-\Gamma_t(f_i))}{2}\right]^2}\right\}, \tag{10}$$

where N is the number of frequency points, $\hat{\Gamma}_m$ and Γ_t are the measured and theoretical coherence values, respectively, and $\Re$ and $\Im$ indicate real and imaginary parts. The normalization condition has been chosen such that the difference function varies between a minimum of 0 and a maximum of

100. Implicit in this normalization is the fact that the range of possible values for the real and imaginary coherence is from $+1$ to -1, meaning that the argument under each square root in Eq. (10) has a minimum value of 0 and a maximum value of N.

The sum over frequency implies equal weighting to all frequency components. This is a reasonable approach provided that the measured coherence contains sufficient structure at all frequencies. There is, however, some physical justification for other weighting functions. For instance, the lower-frequency components could be weighted preferentially over the higher-frequency components because surface scattering, which is unaccounted for in the model, would be more likely to alter the higher-frequency measurements. Or, the imaginary component, which is typically a factor of 2 to 3 smaller than the real component, could be preferentially weighted to account for the difference. Or, coherence values near zero magnitude could be deemphasized because they are more likely to be contaminated by electronic noise. These and other weighting functions may prove useful in future applications of the inversion, but will not be necessary in the current study.

The frequency band chosen for the inversion represents a compromise of the following factors. A low-frequency component is desirable in order to maximize the penetration depth into the sediment. However, focusing on only low frequencies increases the risk of error from shipping-contaminated noise, which is not being modeled here. Higher-frequency components are desirable in order to ensure the use of wind-generated noise and in order to obtain sufficient structure (i.e., zero crossings) in the coherence function. However, very-high-frequency noise is undesirable because it only samples the surficial sediment, and the coherence structure is more likely to be affected by surface scattering. Consequently, the frequency band of 100 Hz to a few kilo-Hertz is chosen to most reliably estimate the upper few meters of seabed using predominantly wind-generated noise. In the inversions results that follow, slight variations on these limits are applied because of hardware limitations imposed during the collection of data.

The inversion procedure is to minimize the norm between the theoretical and measured broadband, complex coherence functions for the three-dimensional parameter space c_{p3}, c_{s3}, and z_s. The source depth is considered as a free parameter here as it is unknown and can affect the higher-frequency components of the coherence.[21] The theoretical coherence functions are computed for a matrix of the three parameters and saved in a look-up table for comparison with the data. The compressional wave speed is varied from 1550 to 2800 m/s, the shear wave speed is varied from 0 to 1400 m/s, and the source depth is varied from 0 to 1 m. The remaining seabed parameters are correlated using the relationships outlined in the Appendix. In the results that follow, the values of the norm are plotted on a two-dimensional (c_{p3} and c_{s3}) ambiguity surface for the source depth where the best fit occurs. The final estimate is the three-parameter combination that provides the minimum value of Eq. (10).

V. INVERSION RESULTS

At this point, we present inversions from two shallow water sites: the Cortes Bank and the North Celtic Sea.

A. The Cortes Bank

The Cortes Bank is a raised bank of volcanic origin located in the California Continental Borderland, 90 nautical miles from Pt. Loma, CA. The shallow area of the bank has a spatial extent of approximately 20 by 30 km. The top of the bank is characterized by large wave cut terraces of exposed bedrock, isolated areas of sediment pooling, and extensive areas of sediment deposits along the slopes. The areas of thin or absent sediment coverage were chosen for the experiment in order to maximize the chances of detecting the sandstone substrate, and measuring the shear speed. The exposed bedrock is composed of consolidated sedimentary and volcanic rock of probable Tertiary age.[22] A generalized geoacoustic model from the neighboring Tanner Bank indicates a variable sediment overburden of 0 to 6 m with bedrock compressional and shear wave speeds of 2500 and 900 m/s, respectively.[23] Because of the proximity and similar geologic origin of the two banks, these parameters should be approximately representative of the Cortes Bank as well.

The experiment was conducted on 28 March 1995 using a 50-ft chartered vessel called the *Osprey*. The *Osprey* was equipped with a downward-looking sonar which was used to help select an experimental area where exposed bedrock was present. The experiment was performed at $32°27.997'\mathrm{N} \times 119°10.454'\mathrm{W}$, in sea state 3, over an approximately 6 by 10-km area of exposed bedrock and in a water depth of 70 m. The receiver separation was 1 m and the hardware contained a low-pass filter at 2500 Hz. The coherence for five time segments is shown in Fig. 7(a). The corresponding spectra (not shown) display a spectral slope of about negative 3–4 dB/oct at the low frequencies, increasing to negative 5–6 dB/oct above 1 kHz.[24] These slopes are typical of wind-generated ambient noise, and suggest that there is little or no contamination from shipping. The five curves shown in Fig. 7(a) were averaged together to provide the final coherence estimate used in the inversion. Because the data were unreliable below 250 Hz, the inversion was performed on the coherence over the frequency band of 250–2500 Hz. The look-up tables were calculated using an isovelocity profile and a homogeneous half-space basement. The theoretical coherence values were computed every 50 Hz, providing $N=46$ frequency points in the coherence curves. The measured coherence was computed using 512-point FFT's and interpolated to the 46 frequency points. The inversion results are shown in Fig. 8 for a source depth of 0.1 m where the best fit occurred. The ambiguity surface indicates a best fit at a value of $c_p=2350$ m/s and $c_s=1150$ m/s. The result is well resolved in the c_p and c_s dimensions and is in reasonable agreement with the model of Bucca and Fulford.[23] The estimates demonstrate that both compressional and shear wave speeds of the exposed bedrock can be measured from the ambient noise coherence.

The compressional wave speed estimate is lower than the 2500 m/s value given by Bucca and Fulford. One explanation for this comes from the depth-averaging property of

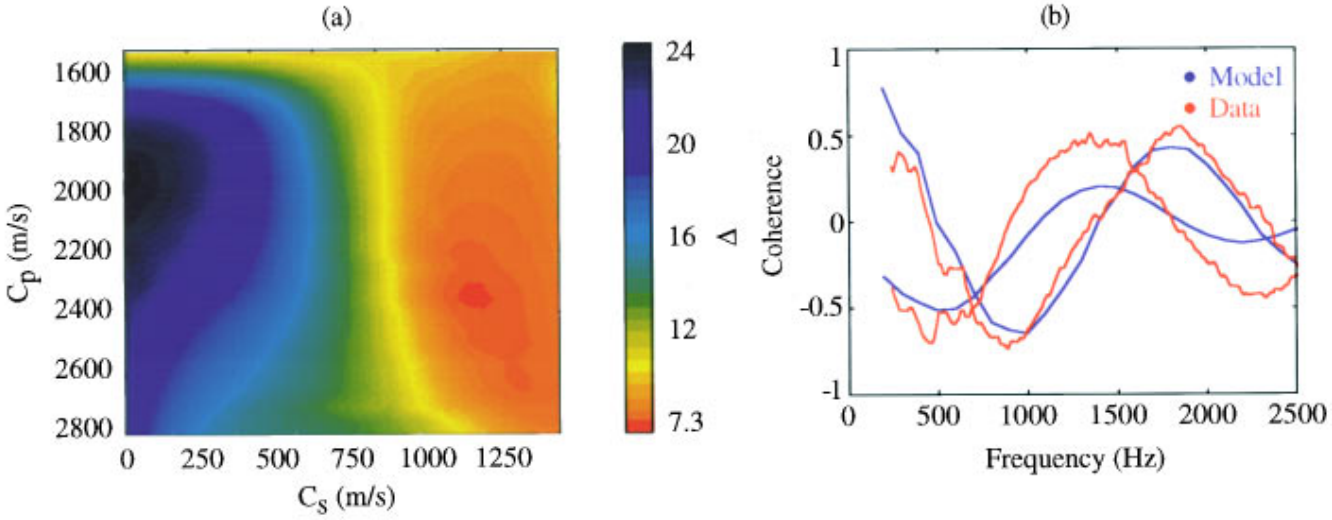

FIG. 8. Inversion result for the Cortes Bank data site. The best fit occurs at $c_p = 2350$ m/s and $c_s = 1150$ m/s for a value of $\Delta = 7.3$.

the ambient noise technique. Since the site consists of exposed bedrock as well as areas of thin surficial sediment over the bedrock, the inversion estimate represents a reasonable average of these material properties. Another factor which might explain the low c_p estimate is the presence of a sound speed profile. A CTD (conductivity, temperature, and depth) cast was taken during the experiment to measure this profile, but the data were not recoverable. It is unlikely that a significant sound speed profile was present because of the turbulent mixing above the bank. However, since the experiment was conducted in the springtime when solar warming of the surface is prevalent, the existence of a weak downward-refracting sound speed profile is a reasonable possibility. To address this possibility, the look-up tables were recomputed assuming a modest downward-refracting profile. A linear profile was used that varied from 1518 to 1500 m/s over the 70-m channel depth. The inversion result showed little change from the isovelocity case. The best fit occurred at $c_p = 2350$ m/s and $c_s = 1200$ m/s. The reason that little change occurred is because the trapped modes were stripped out by the high shear speed basement, such that the noise incurred little additional mode stripping from the sound speed profile. The value of the norm increased from $\Delta = 7.3$ in the isovelocity case to $\Delta = 7.4$ in the downward-refracting case, indicating that the isovelocity profile provides a marginally better fit.

The best fit of the model to the data is also shown in Fig. 8. The real component shows a good fit over the entire frequency band. However, the imaginary component fit is somewhat less precise. The imaginary component of the data shows greater oscillations than the model, particularly at frequencies above 1 kHz. This may account for the high shear estimate, which is strongly dependent on the imaginary component. A possible explanation for the large imaginary component comes from surface scattering which preferentially influences the shorter wavelengths compared to the longer wavelengths. Scattering from the surface or bottom tends to displace low angle energy into high angle energy, which is more rapidly attenuated, and can thus be thought of as an additional loss to the specularly reflected component. The increase in the imaginary component can easily be demonstrated using an exponential scattering model. During the experiment, the sea surface above the Cortes Bank exhibited considerable roughness and irregularity. Consequently, it is very likely that surface scattering contributed to the coherence of the measured field. A better theoretical fit to the measured coherence and a more accurate estimate might be obtained if a proper measurement of the rms surface roughness is included in the model. The omission of surface scattering from the model thus limits the accuracy of the seabed estimates for this site. However, as scattering represents a relatively minor modification which is mostly present at higher frequencies, the Cortes Bank inversions presented here demonstrate the feasibility of using the ambient noise coherence to estimate the shear wave speed over exposed consolidated materials.

B. The North Celtic Sea

The second inversion is presented for a site located in the North Celtic Sea at 51°05′N×08°12′W. This site is characterized by a thin layer of sand over a chalk substrate. In Buckingham[2] the compressional wave speed at this site was inverted for using a low-loss fluid model. The inversion resulted in an erroneously low compressional wave speed estimate, which was attributed to the omission of shear from his model. This was one motivation for investigating the effects of shear in the present study.

An independent survey of the site was performed by measuring the propagation loss from explosive charges to a bottom-mounted array. These measurements were then fitted to the theoretical predictions of a shallow water Pekeris model with an elastic basement. The results are discussed by Ellis and Chapman[25,26] and Staal.[27] In these studies, it was found that the inclusion of shear in the model was necessary to explain the very high losses below 300 Hz. The authors demonstrate good fits to these low-frequency data using typical chalk parameters of $c_p = 2400$ m/s and $c_s = 1000$ m/s, but

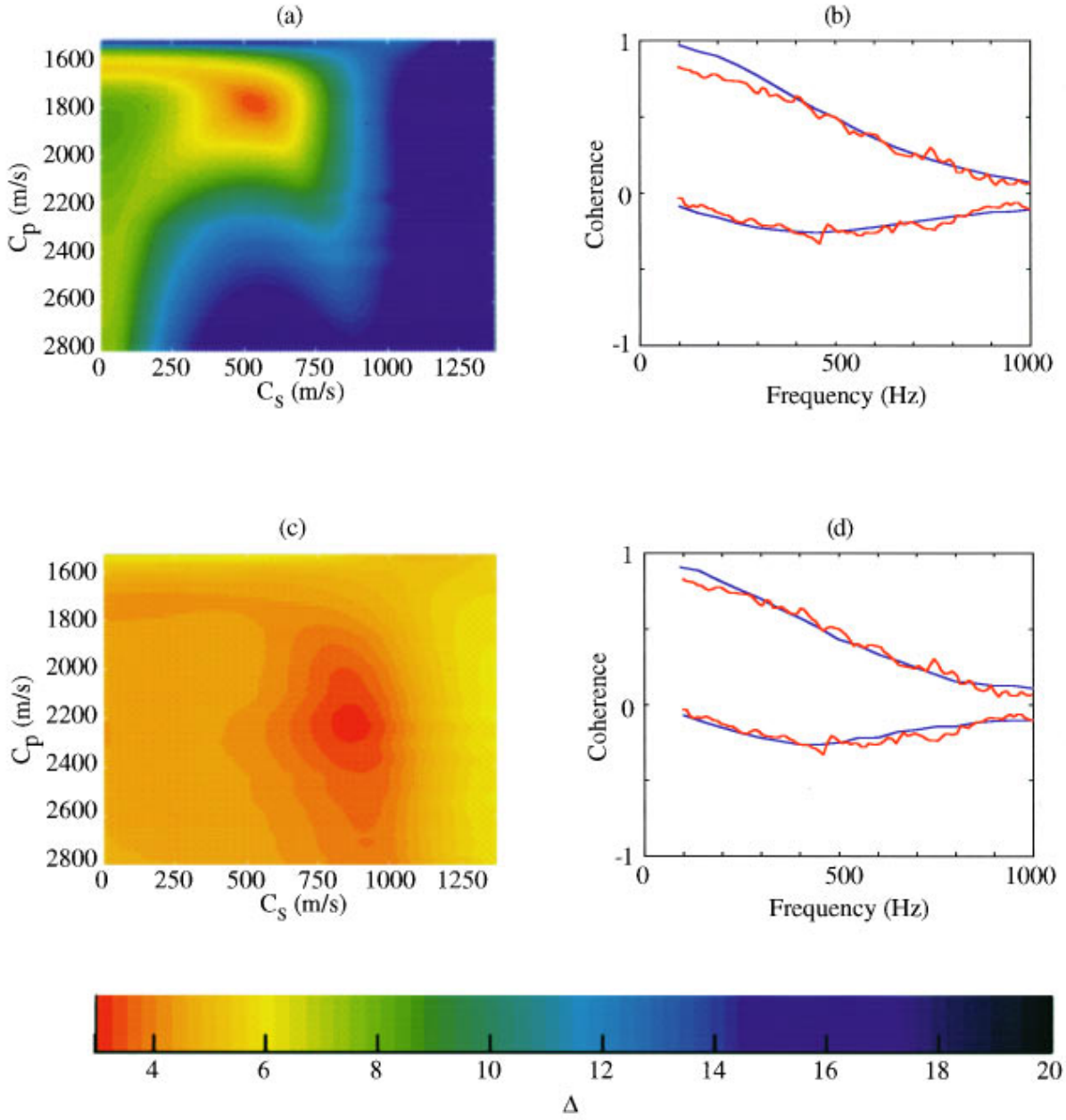

FIG. 9. Inversion results for the North Celtic site using an uncovered half-space bottom and a 1-m layer over a half-space substrate. (a) and (b) are respectively the ambiguity surface and best fit result obtained using the half-space model with no layer. The best fit occurs at 1775 m/s and 525 m/s with $\Delta = 3.1$. (c) and (d) are the ambiguity surface and best fit result obtained using a 1-m layer of sand over a half-space substrate. The best fit for the layered model occurs at 2225 m/s and 875 m/s with $\Delta = 2.9$.

state that better fits were achieved using slightly lower shear speeds. Furthermore, it was determined that the effects of a thin sediment layer, which they modeled as 1 m of sand, were important in the propagation loss measurements above 500 Hz. These estimates will serve as ground truth for the ambient noise analysis.

The North Celtic experiment was performed on 17 July 1983 in a water depth of 104 m. Data were collected for approximately 1 h using sonobuoy arrays described in Ref. 2, which have minimum receiver separation of 1 m and a low-pass filter cutoff of 1 kHz. The conditions during the experiment were sea state 1 with winds below 5 m/s. The spectra and coherence were computed from 2-min segments of data using 512-point FFTs with 50% overlap and a Kaiser–Bessel[20] window $\beta = \pi\alpha = 7.85$. The spectra (not shown) exhibit a slope of -5 dB/oct over the 100–1000-Hz band, but do not display the characteristic wind noise rolloff below 500 Hz.[24] This lack of rolloff and a spectral line at 240 Hz suggest that shipping, or at least fishing vessels, may be a factor in the data.

The theoretical coherence curves were computed for 50-Hz increments, providing $N = 19$ frequency points. The inversion results are shown in Fig. 9 for a source depth of 0.65 m where the best fits occurred. The ambiguity surface and best fit for a receiver pair separated by 1 m are shown in Fig. 9(a) and (b), respectively. The ambient noise estimates using the half-space model are $c_p = 1775$ m/s and $c_s = 525$ m/s. The results are low compared to the measured

values for the chalk substrate. This low estimate can be explained by the thin surficial sand layer that separates the chalk from the water column. The sand inhibits the compressional to shear wave conversion, and the inversion represents an average over the two materials.

For the frequencies used in the inversion we expect the average to represent the upper few meters of seabed. Ellis and Chapman found that a 1-m layer of sand was necessary to fit their propagation loss data above 500 Hz. Based on their findings, the look-up tables were recomputed for a variable homogeneous half-space covered by a fixed 1-m layer of sand. The layered inversion results are shown in Fig. 9(c) and (d). The estimate has moved out in parameter space to $c_p = 2225$ m/s and $c_s = 875$ m/s, which is in good agreement with the independent survey. Furthermore, the value of the norm has decreased from 3.1 to 2.9, indicating that the layered model has provided a marginally better fit.

Figure 9(a) and (c) is plotted on the same color scale. This is done to illustrate that the resolution in parameter space decreases when inverting for subsurface layers. This is not surprising because the noise is dominated by the uppermost sediment, whereas progressively deeper layers have less overall effect. Nonetheless, this result demonstrates the possibility of using ambient noise not only to estimate average seabed parameters, but also to measure a layered structure in the upper few meters. In this case we had the benefit of knowing the surficial sediment composition in advance. In general, when prior information is not available, a more systematic approach would need to be employed.

The results in this section demonstrate the ability of the ambient noise method to extract the seabed parameters, given the appropriate model. It is clear that the measured noise field can be altered substantially by the presence of a thin sedimentary layer. Given no prior knowledge of the seabed structure, this can lead to estimates that represent average seabed characteristics, and possibly estimates that mischaracterize the seabed. At the present time, the technique has not been refined to the point where the process of selecting the appropriate model can be automated. However, the improvement in the fit with the appropriate model selection suggests that such a procedure could be developed based on the minimum norm criterion.

VI. CONCLUDING REMARKS

Using a theoretical model of wind-generated ambient noise, it has been shown that the vertical directionality and vertical coherence of the noise are sensitive to both the compressional and shear wave speeds of the seabed. The compressional wave speed affects the symmetrical part of the noise directionality, which is manifest in the real component of the coherence. The conversion of compressional wave energy in the water column to shear waves in the seabed is a loss mechanism that strips intermediate trapped mode energy from the water column. As such, it decreases the symmetry in the noise and increases asymmetry. This is manifest as a decreased zero crossing in the real component and an increased magnitude in the imaginary component of the coherence.

The time-averaged directionality and coherence are relatively stable features of the noise and are relatively independent of temporal variations in the ocean environment. This has been demonstrated using distinct estimates of the coherence taken over time from two ocean sites. At one site, the structure of the coherence remained stable over a 1-h period while the power spectral density varied by up to 15 dB. At the other site, similar consistency was seen in the measured coherence taken from five separate days while the sea state varied between 1 and 3.

Based on the noise field dependence on the seabed, an inversion procedure was developed to estimate the compressional and shear wave speeds using the broadband coherence from a single hydrophone pair. Estimates obtained from the ambient noise will, by the very nature of ambient noise, represent an average over range and depth. Modeling of the coherence over a layered basement indicates the broadband coherence over the frequency band of 100 to 2000 Hz is determined by the upper few meters of seabed. In addition, a preliminary investigation into a range-dependent noise model indicates that the coherence represents a range footprint of 10–25 km.[24] Although these types of estimates will not be useful in detailed exploration of the ocean seabed, they provide a simple, cost effective means of estimating the average upper seabed properties.

The ambient noise inversion has been applied to ocean data from two shallow water sites. At the Cortes Bank, where the bedrock was exposed, a half-space model of the seabed provided reasonably accurate estimates of the compressional and shear wave speeds. For the North Celtic site, the half-space model proved to be insufficient due to the *in situ* presence of a thin sedimentary layer overlying the chalk substrate. However, by including the sedimentary layer in the model, the parameter estimates of underlying chalk improved significantly. This suggests that, by developing a systematic approach to focus on successive basement layers, the technique may be improved to not only give more accurate estimates, but to also determine a rough sound speed profile for the seabed.

ACKNOWLEDGMENTS

The authors wish to acknowledge the Naval Undersea Warfare Center for providing the data from the Florida Shelf and the Defence Research Agency—Farnborough for providing the data from the North Celtic. In addition, we thank Richard Bachman for supplying seismic profiling information from the Cortes Bank. This work has been supported by the Office of Naval Research under Contract No. N00014-91-J-1118.

APPENDIX: CORRELATION EQUATIONS FOR SEABED PARAMETERS

In the calculation of the coherence look-up tables, only two seabed parameters were held as free variables, c_{p3} and c_{s3}. The compressional wave speed is the primary parameter affecting the coherence, and is always included in the inversion. The absorption and shear wave speed are parameters that trade off in importance depending on whether the seabed

is fluidlike or shear supporting, respectively. For the consolidated seabed materials considered in this study, the loss due to shear outweighs absorption loss. As such, the value of α_{p3} was not included in the inversion, but was correlated with the compressional wave speed according to the following equation:

$$\alpha_{p3}=\{2.64-1.06\times10^{-3}c_{p3}\}\ \text{dB/}\lambda. \tag{A1}$$

The density and shear wave absorption are parameters of limited significance in the coherence calculation. Consequently, they were correlated with other parameters according to the following equations:

$$\rho_3=\begin{cases}\dfrac{b+\sqrt{b^2+4a(c_{p3}-2270.9)}}{2a}\ \text{kg/m}^3, & 1.25\leqslant\rho_3\leqslant2.1,\\ 1.62+2.61\times10^{-4}c_{p3}\ \text{kg/m}^3, & 2.1<\rho_3\leqslant2.4,\end{cases} \tag{A2}$$

where

$$a=474.6,\quad b=1194.4,$$

and

$$\alpha_{s3}=[1.97-1.18\times10^{-3}c_{s3}]\quad \text{m/s}. \tag{A3}$$

In addition to these correlations, lower limits of $\alpha_{p3}=0.05$ dB/λ and $\alpha_{s3}=0.1$ dB/λ were imposed as practical limits.

The correlations above are estimates based on a substantial body of *in situ* research conducted by Hamilton and others. The equations for α_{p3} and α_{s3} are linear fits to correlations found in Jensen *et al.*[19] The quadratic equation correlating ρ_3 with c_{p3} comes from Hamilton,[16] and is valid for the values of ρ_3 indicated. Above $\rho_3=2.1$, a linear fit to *in situ* data is again used.

As the coherence function does not have sufficient structure to resolve all five parameters, these correlations are an attempt to minimize the error that results from not actually knowing their values. Mismatch between the actual *in situ* values and those derived from Eqs. (A2) and (A3) are expected to have negligible effects on the coherence. Errors associated with Eq. (A1), on the other hand, are expected to be most significant when the absorption is largest. This means that shear speed measurements will be uncertain for low compressional wave speed seabeds where the effects of absorption become significant and where absorption levels are more variable in nature.

[1] D. M. F. Chapman, in *Underwater Communication and Position Fixing* (Institute of Acoustics: University of East Anglia, Norwich, England, 1987), pp. 1–11.

[2] M. J. Buckingham and S. A. S. Jones, ''A new shallow-ocean technique for determining the critical angle of the seabed from the vertical directionality of the ambient noise in the water column,'' J. Acoust. Soc. Am. **81**, 938–946 (1987).

[3] R. M. Hamson, ''The modelling of ambient noise due to shipping and wind sources in complex environments,'' Appl. Acoust. **51**(3), 251–287 (1997).

[4] M. J. Buckingham, ''A theoretical model of ambient noise in a low-loss, shallow water channel,'' J. Acoust. Soc. Am. **67**, 1186–1192 (1980).

[5] R. M. Hamson, ''The theoretical responses of vertical and horizontal line arrays to wind-induced noise in shallow water,'' J. Acoust. Soc. Am. **78**, 1702–1712 (1985).

[6] W. A. Kuperman and F. Ingenito, ''Spatial correlation of surface generated noise in a stratified ocean,'' J. Acoust. Soc. Am. **67**, 1988–1996 (1980).

[7] H. Schmidt, *OASES: Application and Upgrade Notes* (MIT, Cambridge, MA, 1994).

[8] H. Schmidt, *SAFARI: Seismo-acoustic Fast Field Algorithm for Range Independent Environments. User's Guide* (SACLANT Undersea Research Centre, La Spezia, Italy, 1988).

[9] C. H. Harrison, ''Formulas for ambient noise level and coherence,'' J. Acoust. Soc. Am. **99**, 2055–2066 (1996).

[10] Z. Y. Zhang and C. T. Tindle, ''Complex effective depth of the ocean bottom,'' J. Acoust. Soc. Am. **93**, 205–213 (1993).

[11] S. O. Rice, ''Mathematical analysis of random noise,'' Bell Syst. Tech. J. **23**, 46–156 (1945).

[12] D. C. Stickler, ''Normal-mode program with both the discrete and branch line contributions,'' J. Acoust. Soc. Am. **57**, 856–861 (1975).

[13] P. Balasubramanian and M. M. Muni, ''A note on 'The effective depth of a Pekeris ocean waveguide, including shear wave effects' [Chapman *et al.*, J. Acoust. Soc. Am. **85**, 648–653 (1989)],'' J. Acoust. Soc. Am. **88**, 564–565 (1990).

[14] H. Cox, ''Spatial correlation in arbitrary noise fields with application to ambient sea noise,'' J. Acoust. Soc. Am. **54**, 1289–1301 (1973).

[15] A. C. Kibblewhite, ''Attenuation of sound in marine sediments: A review with emphasis on new low frequency data,'' J. Acoust. Soc. Am. **86**, 716–738 (1989).

[16] E. L. Hamilton, ''Geoacoustic modeling of the sea floor,'' J. Acoust. Soc. Am. **68**, 1313–1340 (1980).

[17] E. L. Hamilton, ''Compressional-wave attenuation in marine sediments,'' Geophysics **37**, 620–646 (1972).

[18] E. L. Hamilton, ''Sound velocity, elasticity, and related properties of marine sediments, North Pacific,'' Naval Undersea Research and Development Center (1969).

[19] F. B. Jensen, W. A. Kuperman, M. B. Porter, and H. Schmidt, *Computational Ocean Acoustics* (American Institute of Physics, New York, 1994), 1st ed., Vol. 1.

[20] F. J. Harris, ''On the use of windows for harmonic analysis with the Discrete Fourier Transform,'' Proc. IEEE **66**, 51–83 (1978).

[21] M. J. Buckingham and N. M. Carbone, ''Source depth and the spatial coherence of ambient noise in the ocean,'' J. Acoust. Soc. Am. **102**, 2637–2644 (1997).

[22] H. G. Greene, S. H. Clarke, Jr., M. E. Field, F. I. Linker, and H. C. Wagner, ''Preliminary report of the environmental geology of selected areas of the Southern California Continental Borderland,'' United States Department of the Interior Geological Survey (1975).

[23] P. J. Bucca and J. K. Fulford, ''Environmental variability during the Tanner Bank Phase of the Pacific Coast Operation,'' Naval Research Laboratory (1995).

[24] N. M. Carbone, ''Inverting for geoacoustic seabed parameters using ambient noise,'' Ph.D. Thesis, University of California at San Diego, Scripps Institution of Oceanography, 1996.

[25] D. D. Ellis and D. M. F. Chapman, ''Modelling of shear-wave related acoustic propagation on the U.K. continental shelf,'' DREA (1984).

[26] D. D. Ellis and D. M. F. Chapman, ''A simple shallow water propagation model including shear wave effects,'' J. Acoust. Soc. Am. **78**, 2087–2095 (1985).

[27] P. R. Staal, in *Acoustics and the Sea Bed*, edited by N. G. Pace (Bath U.P., Bath, England, 1983), pp. 289–296.